Urbanization exacerbates intensification of short-duration rainfall extremes in a warming climate

Haochen Yan[1], Yao Gao[1,2], Robert Wilby[3], Dapeng Yu[3], Nigel Wright[4], Jie Yin[5], Xunlai Chen[6], Ji Chen[1], Mingfu Guan[1*]

[1] Department of Civil Engineering, the University of Hong Kong, Hong Kong SAR

[2] Finnish Meteorological Institute, Helsinki, Finland

[3] Geography and Environment, Loughborough University, Loughborough, UK

[4] School of Engineering, University of Birmingham, UK

[5] Key Laboratory of Geographic Information Science (Ministry of Education), East China Normal University, China

[6] Shenzhen Meteorological Bureau, Shenzhen, China

Corresponding to: Dr. Mingfu Guan, Assistant Professor in Hydro-environment and Geohazard (mfguan@hku.hk)

Key Points:

- Spatially distinct and nonlinear increase of sub-daily rainfall extremes are revealed over a rapidly developing coastal megalopolis
- Short-duration intensification is prominent in urban areas as apposed to rural areas exhibiting less timescale-dependent variability
- More frequent nuisance hourly-scale events are expected in urban areas while daily-scale events nominally increase with return period

Abstract

Intensification of short-duration rainfall extremes is posing greater urban flood risk. Yet, it remains intriguing how the upper-tail statistics update with regional warming. Here, we characterize the non-stationarity of rainfall extremes with durations from 1 to 24 hours over a rapidly developing coastal megalopolis, namely the Greater Bay Area in China, using multi-source merged gridded data of high spatiotemporal resolution. We observe prominent increasing rainfall intensities particularly for the north-central part of the region as opposed to the southern coastal region. Our results show, for the first time, that urbanization nonlinearly exacerbates the rainfall intensities at different extremities, which favors short durations (≤ 3-hour) and short return periods (2-year), with remarkably high return level-based scaling rates (> 34%/°C). Conversely, rural areas exhibit higher scaling rates than the urban areas for longer durations (≥ 9-hour), with lower degree of dependency on both durations and return periods.

Plain Language Summary

Short-duration (sub-daily) rainfall extremes, a major driver of flash floods, are disruptive to humans and societies. It is widely recognized by both numerical and statistical studies that urbanization intensifies short-duration rainfall extremes. However, little work provides regional quantification of the rate of intensification under a warming climate, particularly regarding the extreme quantiles that correspond to the return periods comparable to or even longer than the data time span. In this study, we take one of the world's most famous and urbanized bay areas as an example. The high spatiotemporal-resolution dataset of a 30-year time span merged from gauge networks, satellite observations, and reanalysis products, enables spatially continuous and coherent analysis of low-frequency extremes (2- to 100-year return levels) under a novel nonstationary framework that incorporates the association with changing climate. The results highlight the essential control of timescales on rainfall extremes intensities particularly in urban areas in contrast to rural areas, as well as a higher rate of magnification of short-return period events, suggesting more 'nuisance' rainfall with the increasing surface temperature. This study offers a new perspective/framework for climate risk assessment and urban flood adaptation under a changing climate.

1 Introduction

Heavy precipitation has increased in intensity and frequency for most land areas since the 1950s – trends that have been attributed to human-induced global warming (IPCC, 2021). Whilst such changes at daily or longer durations are detected globally (IPCC, 2021; Papalexiou & Montanari, 2019; Westra et al., 2013), sub-daily rainfall extremes, which can cause severe socioeconomic impacts through flash flooding (Ayat et al., 2022; Fischer & Knutti, 2016; Fowler et al., 2021), generally exhibit much greater variability across continents, regions, and sites (Agilan & Umamahesh, 2015; Barbero et al., 2017; Y. Chen et al., 2021; Fowler et al., 2021; Hosseinzadehtalaei et al., 2020). In urban areas, where more than half of the world's population is concentrated (Grimm et al., 2008), rainfall patterns are modified due to i) heat island, ii) higher roughness, iii) higher aerosol concentration and iv) anthropogenic infrastructures, which collectively enhance the extreme and total rainfall locally and downwind (Han et al., 2014; J. Liu & Niyogi, 2019; Shepherd, 2013). Hence, continuous and rapid urbanization is placing more areas under rising flood risk especially in the economic growth hubs in the Asia-Pacific region.

Extreme value theory (EVT) is typically used to evaluate the statistical properties of rainfall extremes, which then enables extrapolation to events outside the range of available data (Khaliq et al., 2006). Associated methodologies such as intensity-duration-frequency (IDF) curves are routinely applied to infrastructure design and water management (Hosseinzadehtalaei et al., 2020). However, these conventional techniques rest on the assumption of stationarity which is problematic in the context of climate change, as the probability distribution of the extreme variable studied is time-invariant (Khaliq et al., 2006; Milly et al., 2008). Hence, as seen worldwide (Fauer & Rust, 2022; Fu et al., 2021; Slater et al., 2021; Vu & Mishra, 2019), it makes sense to consider the non-stationarity of rainfall extremes using EVT. However, rain gauge networks, which are often relied upon for extreme value analysis, have uneven and sparse coverage and may under- or mis- sample convective events which largely contribute to short-duration extremes (Kidd et al., 2017; Lengfeld et al., 2020). On the other hand, satellite-derived or analysis-based gridded precipitation products offer fine spatiotemporal resolutions and complete coverage (Q. Sun et al., 2018). Nevertheless, they are inadequate for regional extreme value analysis due to significant uncertainties in their accuracy (Alexander et al., 2019; Ali et al., 2021; J. Zhang et al., 2022). In this regard, blending the merits of multiple sources for long-term rainfall statistics characterization is recommended, e.g., the studies on urban rainfall effects (McLeod et al., 2017; McLeod & Shepherd, 2022), while hourly non-stationarity studies with blended datasets remain rare.

Increasing intensities of sub-daily rainfall in urbanized areas are detected by nonstationary EVT based on one or a few scattered station (Agilan & Umamahesh, 2015; Ganguli & Coulibaly, 2017; Yilmaz et al., 2014) (Fig. S1, Table S1), whereas cross-duration features and coherent spatial patterns that quantify rural-urban contrasts are still unclear. The statistical relations between the non-stationarity and underlying climate drivers, implied by time and physical covariates formulated in frequency models, further complicate takeaway messages for decision-makers in the context of growing urbanization and surface temperature (Y.-R. Chen et al., 2013; Fauer & Rust, 2022; Westra & Sisson, 2011). Many studies have applied Clausius-Clapeyron (C-C) scaling to examine how the moisture-holding capacity of the atmosphere and thus rainfall intensity responds to global warming (Bao et al., 2017; Lenderink & van Meijgaard, 2008; Visser et al., 2021; Westra et al., 2014) relating extreme quantiles to incremental temperature bins, usually under daily timescale (Fowler et al., 2021). However, the scaling for the 'upper tails' of short-duration rainfall intensities (return periods well beyond the length of observational records) indicative for the non-stationarity is hitherto unexplored.

Here, we analyze the non-stationarity in hourly to daily rainfall extremes (with intensities ≥2-years return period) in relation to surface temperature over the Greater Bay Area (GBA). The GBA is an agglomeration of 11 metropolitan areas in south China covering Guangdong, Hong Kong and Macau. This region has experienced a surge of urban development and population growth since the 1990s, becoming the most important economic hubs in Asia (Qiang et al., 2020; X. Sun et al., 2021). Moreover, it is one of the most vulnerable urban areas globally, given its high exposure to floods, dense population, and developing economy (Schelske et al., 2013). Having differentiated areas with high and low degrees of urbanization, we investigate the non-stationarity of rainfall extremes over the region over hourly to daily scales with potential climate drivers being assessed; robust scaling relation regarding the detected nonstationary for the timescale-dependent upper-tail statistics are also proposed and demonstrated.

2 Materials and Methods

2.1 Meteorological data and multisource merging

This study applies nonstationary frequency analysis to high-resolution hourly rainfall data. The gridded rainfall data include Multi-Source Weighted-Ensemble Precipitation (MSWEP V2.8) (Beck et al., 2019), Integrated Multi-satellite Retrievals for the Global Precipitation Measurement mission (IMERG) Final Run Version 07 (Huffman et al., 2023), and the ERA5-Land reanalysis data of European Center for Medium-Range Weather Forecast (ECMWF) (Hersbach et al., 2020). In addition, the rain gauge data from 50 weather stations managed by the National Meteorological Information Center of the China Meteorological Administration and The Hong Kong Observatory are also analyzed. Other meteorological data, covering the period of 1960-2020, include global (land + ocean) mean surface temperature, Multivariate ENSO Index (MEI), mean surface temperature (T2m), mean dew point temperature (DT2m), and mean equivalent potential temperature (EPT). T2m and DT2m data are obtained from the ERA5-Land dataset whereas EPT is calculated following the methods in Song et al. (2022).

2.2 Multisource merging and correction of the gridded rainfall data

The quality assessment of several popular gridded rainfall products around the GBA indicates a poor agreement with gauge observations at the hourly timescale (Fig. S2). Although preliminary calibration has already been performed for the multi-source merged products such as MSWEP, only a limited number of gauges with daily data are adopted (Beck et al., 2019; Hersbach et al., 2020). Thus, we further employ a Random Forest (RF) based Merging Procedure (RF-MEP) (Baez-Villanueva et al., 2020) of the original datasets from multiple resources in Section 2.1 to improve the spatiotemporal accuracy at an hourly 0.1° resolution. The RF-merged dataset significantly outperforms the original datasets in terms of Nash–Sutcliffe efficiency (NSE) coefficient while preserve the spatial variability that the sparse gauge network does not possess (Supporting Text S1, Fig. S2).

2.3 Nonstationary frequency analysis of rainfall extremes

Annual maximum rainfall intensities for each grid/station under various durations are extracted for the frequency analysis. 'Rainfall extremes' refers to the rainfall intensities corresponding to ≥ 2-year return periods. This criterion is roughly equivalent to 98.75th and 99.7th percentiles in terms of event-based and direct sampling from the hourly time series, respectively. The generalized extreme value distribution (GEV) is applied with flexible location and scale parameters with climate variables as physical covariates to take into account the potential non-stationarity (Coles et al., 2003; Nerantzaki & Papalexiou, 2022). Details of the model structure, model selection and parameter estimation are given in Supporting Text S2. Mann-Kendall (M-K) trend analysis with Sen's slope estimator (Gocic & Trajkovic, 2013; Khaliq et al., 2009) is performed for each location/grid for different return levels. In addition, the statistics for the urban and rural areas are compared (Supporting Text S3); the sensitivity of potential climate drivers, regarding mesoscale convective systems, tropical cyclones, and monsoonal activities, are evaluated (Supporting Text S4).

2.4 Surface temperature scaling of nonstationary return levels

To determine how rainfall extremes respond to the regional warming, we calculate the scaling of rainfall intensities at different return levels (RL) with respect to annual mean surface temperature, or the NS-RL scaling for simplicity. Such relation, possibly for the first time, attempts to bridge the rainfall intensities corresponding to a certain exceedance probability under the changing climate with an easily accessible and less uncertain climate variable (i.e., annual mean surface temperature). Similar to the scaling in the time domain (Bao et al., 2017; Lenderink & van Meijgaard, 2008; Visser et al., 2021), the NS-RL scaling assumes that changes in annual mean surface temperature ΔT causes $\alpha\%$ changes in rainfall extremes intensities, such that:

$$P_{2,\mathrm{T,RL}} = (1 + 0.01\alpha)^{\Delta T} P_{1,\mathrm{T,RL}} \tag{3}$$

where $P_{1,\mathrm{T,RL}}$ and $P_{2,\mathrm{T,RL}}$ are the average rain rate at a certain RL of a certain duration (T) of periods 1 and 2, respectively, while ΔT is the difference of the mean annual surface temperature of the corresponding two periods. Simplification of the above equation yields:

$$\alpha = \left[\frac{ln(P_{2,\mathrm{T,RL}}/P_{1,\mathrm{T,RL}})}{\Delta T} - 1\right] \times 100 \tag{4}$$

We apply bootstrapping for the calculated RLs at each grid, specifically, we randomly sample the years analyzed into two subperiods of the same length. Then the median of $\alpha\%$ among all the repetitions are recorded as the representative scaling rate of the grid.

3 Results

3.1 Non-stationarity reflected by annual trends and the duration-dependency

Overall increasing trends are detected for both the annual maximum (AM) and extreme frequency (EF) of 10-year hourly rainfall intensities at gauge stations in the GBA (Fig. 1a-b). For the hourly duration, more than 60% of the stations show positive trends, primarily in the central part of the region. While for the daily duration, less than 50% of the stations have positive EF trends (Fig. 1c-d). Only a few stations (12% for hourly and 10% for daily durations) have significant trends ($\alpha \leq 0.05$) for AM, suggesting a large uncertainty to directly use AM to reflect the non-stationarity, while more stations indicate higher significance levels in terms of EF. Guangzhou (the north-central part of the GBA) has the most rapid changes in rainfall extremes at both hourly and daily scales. Here, trends for hourly and daily intensities are around +15%/10yr for AM, and around + 7%/10yr for EF. In contrast, Zhuhai, Shenzhen, and Hong Kong, which are closest to the coast, have a negative trend for both AM and EF. The non-stationarity analyzed (Fig. 1e-g) using the merged gridded dataset is spatially consistent with the gauge-based results. For the 10-year return period, the maximum trend (+12.2%/10yr) (95% CI [11.7, 12.7]) for hourly rainfall is in central Guangzhou, comparable positive trends also occur at northwestern Huizhou (Fig. 1f1&f4). Negative trends in daily extremes around the southern coastlines (Zhuhai, Shenzhen, and Hong Kong) reach -20%/10yr. In addition, the southwest and the east parts show a low degree of non-stationarity. If stationary models are still applied, the errors (discrepancies from current-stage nonstationary results, calculated based on the covariates in 2020) spatially agree with the nonstationary patterns (Fig. S3). It is worth noting that the clusters subject to severe increasing intensities tend to locate northeast of the core urban regions (Fig. S4), which could be induced by the downwind shift of rain centers by urban areas under prevailing southwesterlies and sea breezes (Han et al., 2014; Shepherd et al., 2010; Shepherd, 2013; X. Sun et al., 2021; Yang et al., 2021).

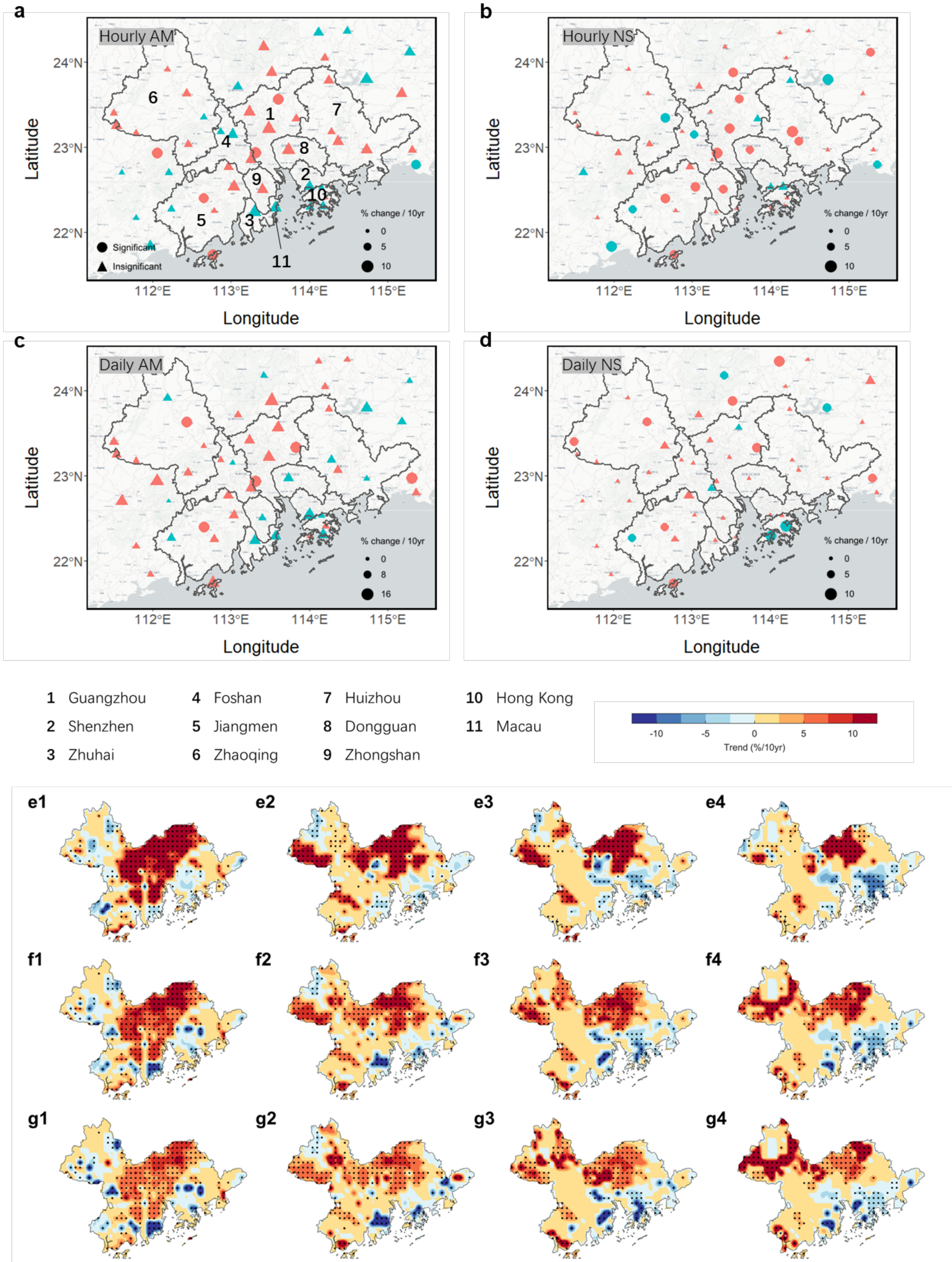

Fig. 1. Nonstationary short-duration rainfall extremes detected by gauge stations and multisource-merged gridded data. The trend in annual maximum rainfall intensity for 1-hour (**a**) and 24-hour (**c**) durations normalized by the mean intensities, and the trend in extreme frequency of 10-year return period rainfall intensity for 1-hour (**b**) and 24-hour (**d**) durations normalized by stationary model results. **e1-g4,** spatially uneven nonstationary rainfall extremes given by the trend normalized by the stationary model results at 2- (**a**), 10- (**b**), and 100-year (**c**) return levels for 1-, 6-, 12- and 24 h durations (subscripts 1-4). Dots mark grids with significant trends ($\alpha \leq 0.05$).

We observe distinct spatial- and duration-dependent (Fig. 1 e-g) patterns of the non-stationarity. From the hourly to the daily durations, the clusters of high-degree non-stationarity tend to shrink and move northward; the fraction of area with stationary rainfall extremes (i.e., low significance level of non-stationarity) also expands. North-central and eastern Guangzhou and northwestern Huizhou exhibit consistent increasing intensities for all return periods and durations, while negative-trend clusters intrude towards inland from the southern coastlines especially for long durations (12- to 24-hour). Accordingly, as the duration increases, less grids are detected to favor nonstationary models (Fig. S5) despite the punishment of Akaike Information Criterion (AIC) score due to the increasing number of model parameters (Supporting Text S2); all the cities except Zhaoqing and Jiangmen, both at western GBA, prefer nonstationary models to the stationary one (Fig. S6). Nonstationary models are almost (>98% of the grids) always preferred rather than the stationary one purely based on AIC, for all the durations (Fig. S5).

3.2 Controls of urbanization degree

The GBA has experienced rapid urbanization, where the urban land cover fraction increased from 5% in 1980 to 15% in 2018 (Fig. S4). Remarkably higher rates of mean annual air temperature ($\overline{T_y}$) during 1991-2020 (P2) are observed compared with 1960-1990 (P1) (Fig. 2a). The classified rural and urban grids have similar trends of $\overline{T_y}$ (+0.080°C/10yr and +0.084°C/10yr in P1, +0.243°C/10yr and +0.237°C/10yr in P2, for urban and rural areas respectively). However, outstanding differences in rainfall extremes between the rural and urban groups can be observed across different durations (Fig. 2b). The urban group sees larger trends than the rural group for short durations (1-2 hours), while the relationship is reversed for longer durations (6-24 hours), and the 3-hour duration appears to be a threshold for such rural-urban contrast. Furthermore, the trends in P2 are consistently larger than those in P1, in align with the trends of mean surface temperature.

The regional non-stationarity viewed from the mediant of 10-year intensity of all grids in the corresponding groups (Fig. 2c-e) agree with the mean statistics in Fig. 2b. Interestingly, during P2, the 1-hour 10-year rainfall intensity increases at a rate much faster in urban areas (+1.88 mm/hr/10yr, 95% CI [1.79, 1.96]) than in rural areas (+0.94 mm/hr/10yr, 95% CI [0.90, 0.98]) (Fig. 2c). However, the discrepancy reduces at the 6-hour duration (Fig. 2d), and then reverses at the 24-hour duration (+0.045 mm/hr/10yr, 95% CI [0.001, 0.009], versus +0.210 mm/hr/10yr, 95% CI [0.195, 0.226], Fig. 2e). The above results educe the necessity to differentiate time scales according to the degree of urbanization when considering long-term flood risk assessment at regional or larger spatial scale.

3.3 Changes in potential climate drivers

The sources of rainfall extremes non-stationarity are likely contributed by changing atmospheric conditions at local, regional and global scales (Slater et al., 2021). Heavy rainfall events mainly occur over southern China during the East Asia summer monsoon (MS) and tropical cyclone (TC) landfall (Lai et al., 2020; Tang et al., 2021). In the Pearl River Basin where the GBA is located, mesoscale convective systems (MCS) contribute to a significant portion of rainfall extremes during monsoons, particularly for the Pre-Meiyu and Meiyu period (mainly in May and June) when southwesterlies prevail (D. Chen et al., 2019; Cheng et al., 2022). We identify the rainfall extremes ($\geq 99^{th}$ percentiles) of each grid in association with one of the five groups of associated climate activities, namely TC, MCS during summer and fall-to-early winter MS periods, and other activities during the two MS periods, and repeat the nonstationary frequency analysis while excluding the AM associated with each type individually (Methods see Supplementary Text S4). We find that summer MCSs and TCs contribute the most (> 10%) to the stationary return level for 1-hour and 24-hour durations (Fig. 2f-h), respectively, and they are comparably important for the 6-hour duration, consistent with the typical lifetime of the associated weather systems (P. Li et al., 2020; L. Liu & Wang, 2020). Summer MSs also contribute non-negligibly for the three durations (1-5%). While TCs account for a larger fraction of rainfall extremes for longer durations (increases from 18% to 34%, from 1-hour to 24-hour durations), the trend of the percentage contribution gradually decreases. Although slowdown of TCs and increasing stalling frequencies are expected to bring higher total precipitation to costal region such as the Pearl River Delta (Hall & Kossin, 2019; Lai et al., 2020; L. Zhang et al., 2023), we also observe a decreased total duration of TC-induced rainfall extremes in the GBA (Fig. S7) align with the decreased contribution to the occurrences of rainfall extremes ($\geq 99^{th}$ percentiles), consistent with the declining TC frequencies under global warming (Chand et al., 2022) particularly in low latitudes (Yamaguchi et al., 2020). Pronounced growing contribution of summer MS to rainfall extremes particularly in urban area is observed, suggesting that smaller-scale convective systems as well as monsoonal activities increasingly influence the non-stationarity. In fact, meso-β- to meso-γ- scale storms (2-200 km) constitute a considerable portion of extreme rainfall events in the GBA (X. Sun et al., 2021), but are likely to be incorporated in the MS group due to the resolution limitation of the gridded infrared brightness temperature data (4-30 km) (Cheng et al., 2022; X. Huang et al., 2018). In addition, the change of contribution of MCSs is relatively milder, and fall-to-early winter activities remain a stable contribution. Besides the 10-year return period presented above, similar patterns are found for 2-year (Fig. S8) and 100-year (Fig. S9) return periods albeit the confidence interval expands with the return period.

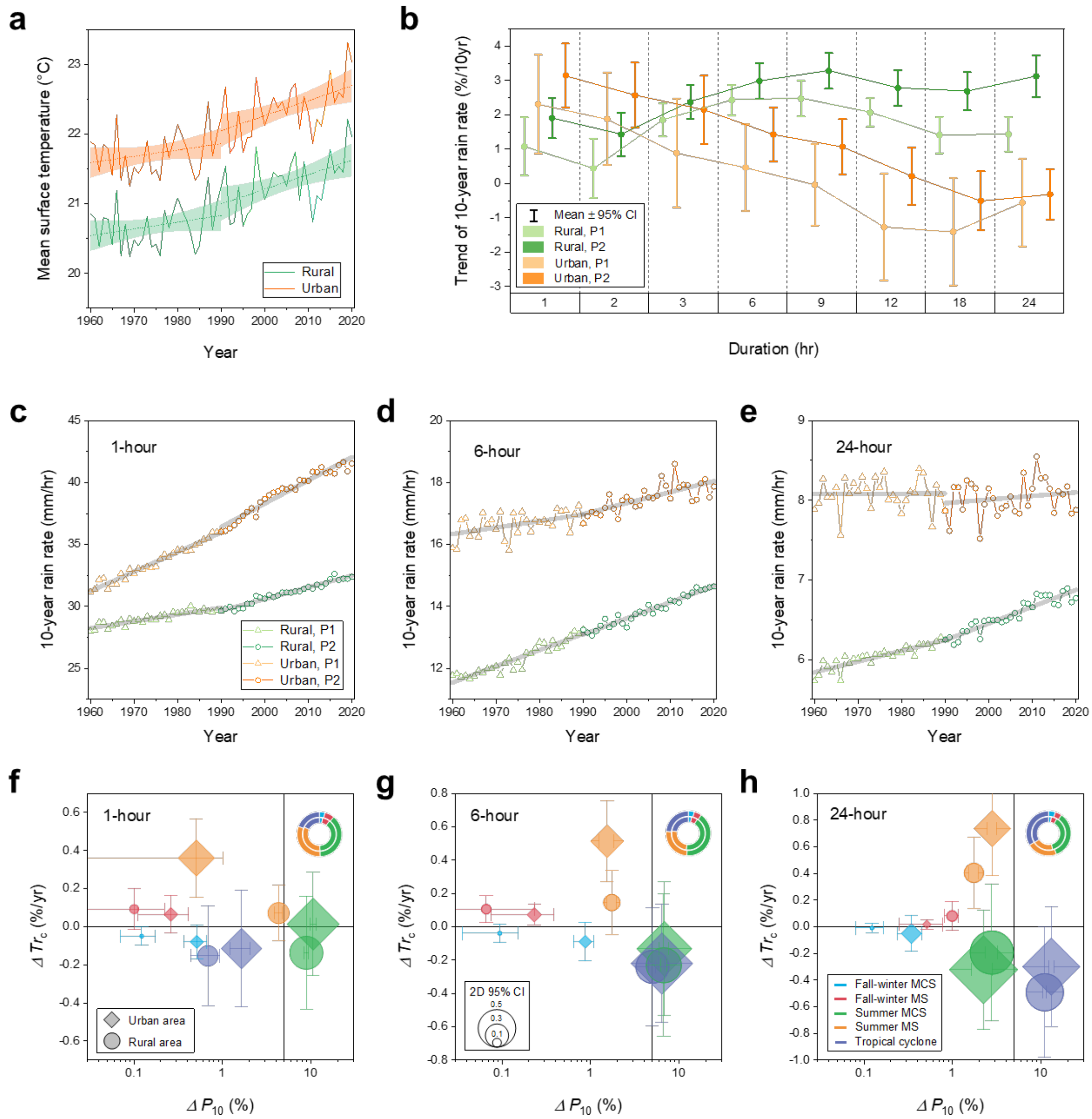

Fig. 2. Non-stationarity in rainfall extremes distinguishing urban and rural areas, and sensitivity to potential climate drivers (10-year return level). a, the median surface temperature time series and fitted linear curves over the rural and urban areas for Period 1 (1960-1990) and Period 2 (1991-2020). **b,** trends at different durations for rural and urban groups. **c-e,** the median rainfall intensity and linear trends for rural and urban areas in Period 1 and Period 2 for 1-hour, 6-hour, and 24-hour durations, respectively. **g-h**, Sensitivity of different climate activities on the 10-year return level. ΔP_{10} is the percentage deviation of mean 10-year return level of the tested group from the results including all the activities; ΔTr_c is the annual trend of the percentage contribution to rainfall extremes. The Doughnut Charts to the top-right corner show the 30-year averaged percentage contribution of each climate activity group, with inner and outer circles showing rural and urban areas, respectively.

3.4 Temperature scaling of the regional non-stationarity

Nonstationary rainfall intensities for various return periods are scaled with the mean annual surface temperature to obtain the NS-RL scaling (Section 2.4). The overall scaling rates vary around the C-C (~ 7%/°C) and super C-C rate (14%/°C), peaking at 1-hour (30%/°C), 6-hour (16%/°C) and 24-hour (13%/°C) durations for 2-year, 10-year and 100-year return periods respectively, with pronounced rural-urban contrasts (Fig. 3). Urban areas peak at 1-hour duration, reaching nearly 40%/°C (highest for all the cases) and maintaining about 34%/°C at the 3-hour duration, and tends to decay for longer durations and return periods. Conversely, rural areas see the peaks equal to or longer than 9-hour duration with smaller variabilities among all the durations. Although short-duration scaling rates tend to decay with an increasing return period as well, they even see an increase for the longer durations (>12 hours). This pattern (Fig. 3) agrees well with the scaling rates directly calculated based on the regional median rainfall intensities (Fig. S10). In addition, most (80%) of the urbanized area in the GBA is in the low-lying region (elevation <60 m) (Fig. S6), such that the inherent elevation and temperature differences between the urban and rural areas may entangle with the effects of land cover. We thus re-calculate the scaling rates excluding the grids with an elevation >100 m (remaining 62% of the entire area). The results show marginal differences in terms of scaling rate magnitudes and rural-urban contrasts (Fig. S11), underlining the role of land cover conditions in the sub-regional differences in the NS-RL scaling.

Although the NS-RL scaling does not adopt event-associated temperature as the C-C relation, its remarkably large variabilities across time scales and the sensitivities to land cover conditions signify strong dynamic controls rather than thermodynamic conditions (Berg et al., 2013). While a higher temperature range is generally favorable for convective precipitation (Fowler et al., 2021), negative slopes of temperature-precipitation scaling are widely observed when temperature exceeds a certain threshold (Berg et al., 2013; Oh et al., 2021; Visser et al., 2021), which can be explained by the lack of moisture availability as relative humidity decreases (or saturation deficit increases) at high temperatures (Chan et al., 2016; X. Sun & Wang, 2022). Because urban areas have higher base temperature than the rural areas (Fig. 2a), longer-duration events in the urban area are more susceptible to such humidity limitation compared to the rural area, leading to a much smaller scaling rates under the same rate of regional warming (Fig. 3). The negative contribution of urbanization on daily-scale precipitation extremes, attributed to the urban dry island effects, are observed in many China coastal urban agglomerations including the GBA (Lin et al., 2020), in contrast to the enhancement for short-lived rainfall extremes by the urban heat island effects (Chang et al., 2023; J. Huang et al., 2022; Y. Li et al., 2020). In addition, the downwind effects (Section 2.1) of urbanization add further complexities to the scaling pattern due to potential nonlocality of the non-stationarity, and the distance depends on organization degree of convection (Naylor & Mulholland, 2023). An improved understanding of the underlying dynamics in control requires the differentiation of rain types in association with atmospheric dynamics at event-based level.

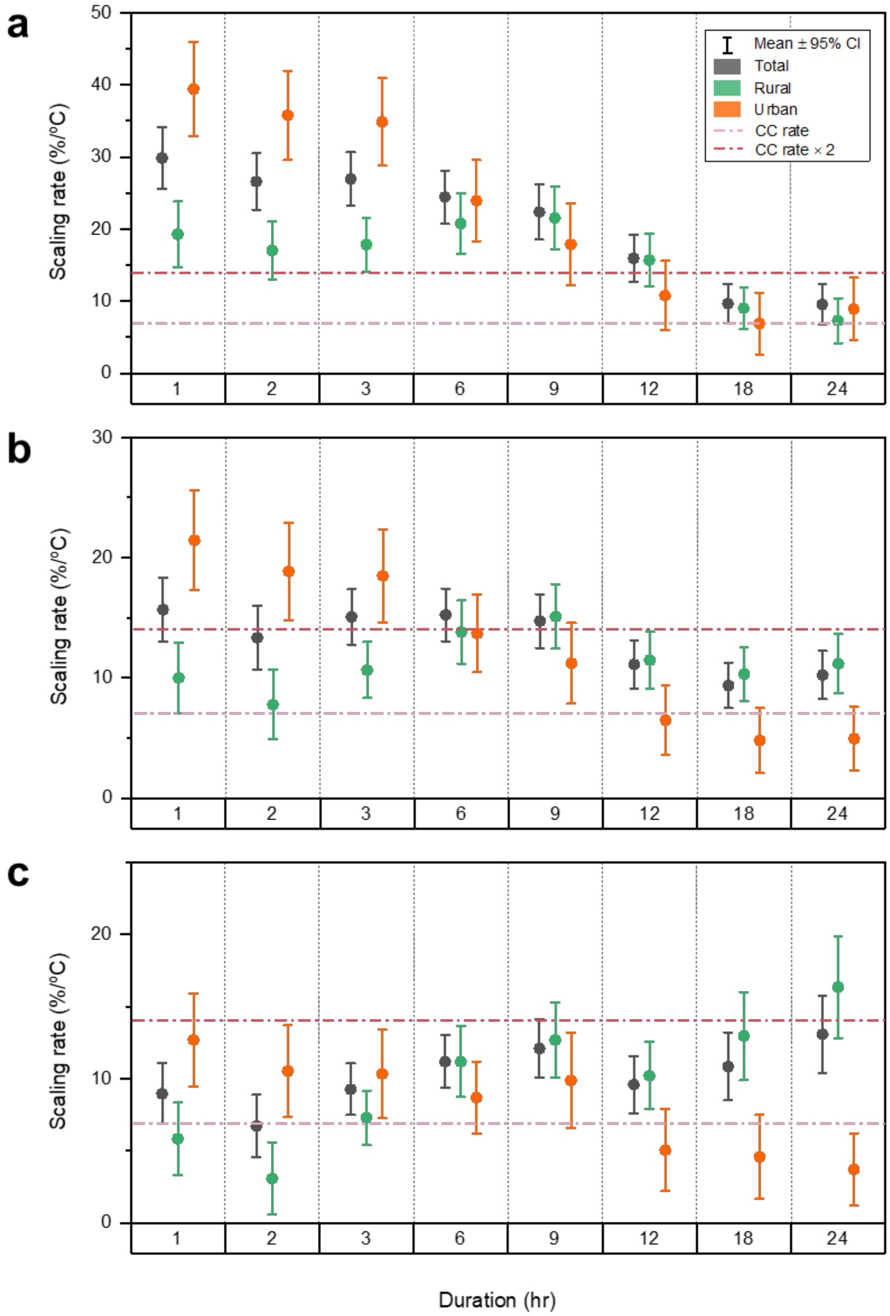

Fig. 3. NS-RL scaling rates for (a) 2-year, (b) 10-year and (c) 100-year return periods. Light and dark dashed lines denote the C-C scaling rate (7%/°C) and super C-C rate (14%/°C, or C-C×2), respectively.

4 Discussion and Conclusion

Our study demonstrates cross-timescale and space-continuous non-stationarity of rainfall extremes over a rapidly developing megalopolis. We detect more severe rainfall extremes over the north-central region of the agglomerations as opposed to the southern coastlines. We also reveal the major contribution by urban areas to the positive non-stationarity for short-duration (< 6-hour) extremes in contrast to more uniform uplift for all durations in the rural areas. These findings are further supported by the temperature-scaling performed for different return levels. Remarkably high short-duration scaling rates in urban areas, which are then waning with increasing durations, highlights the exacerbation of the rainfall extremes by urbanization at short time scales, on top of the overall intensification under the warming climate.

Disputes naturally arise in previous studies regarding the yes-or-no questions – whether the rainfall extremes have nonstationary frequency, and whether to adopt nonstationary models to correct or refine local climate characterizations for infrastructure design (Agilan & Umamahesh, 2016; Ganguli & Coulibaly, 2017; Sarhadi & Soulis, 2017; Vu & Mishra, 2019; Westra et al., 2014; Yilmaz et al., 2014). However, the duration-dependent and spatially nonuniform nature of the non-stationarity (e.g. Fig. 2b&3) presented by our study discourages an oversimplified answer considering the scale-dependent behaviors, which are essential factors to determine both flood risk and effectiveness of flood-protection measures (Yan et al., 2023). At the regional scale (~ 100 km), the ensemble of all the grids exhibits different extent of non-stationarity for urban and rural subgroups shown by the annual trends (Fig. 2b) and integrated in the NS-RL scaling (Fig. 3). At the local/grid scale (~ 10 km), significant spatial disparities exist (Fig. 1e-g), leading to distinct strategies to update IDF curves, for example, a clockwise rotation of IDF curves is expected in Shenzhen and Hong Kong, as opposed to Dongguan, while those of Guangdong may see an overall uplift. Additionally, meter-scale results (based on the gauges, shown in Fig. 1b&d) also deviate from the grid-scale ones, their representativeness in regional climatology should be evaluated upon the spatial scales applied. In brief, with the non-stationarity being perceived as a general case including the stationarity, we recommend depictions for the upper-tail statistics distinguishing the spatial and temporal scales of interest.

This study is among the first to apply a multi-source merged and high spatiotemporal-resolution rainfall dataset to nonstationary frequency analysis, which avoid the drawbacks of sparse, localized, and uneven rain gauge coverage (Kidd et al., 2017; Lengfeld et al., 2020), the poor accuracy of satellite and reanalysis datasets (Alexander et al., 2019; Ali et al., 2021), and the high computational costs and input uncertainties of numerical weather model experiments (Alexander et al., 2019; X. Sun et al., 2021). However, finer-scale extreme events due to deep convection systems (~ 1km) (Lengfeld et al., 2020; Shepherd et al., 2002), as well as highly localized short-duration, slow-moving storms around urban agglomerations (X. Sun et al., 2021), may still be missed by our blended dataset. Radar data are needed to capture the characteristics of sub-hourly rainfall extremes at 1 km resolution (Ayat et al., 2022; Lengfeld et al., 2020), but are not applied in this study due to unavailability for a long time span (> 20 years). This challenge is not unique to the Greater Bay Area and is a global challenge (Lengfeld et al., 2020). Future efforts to investigate such small spatiotemporal-scale extremes are imperative, which can be assisted by denser rain gauge networks (Kidd et al., 2017), radar reflectivity measurements (Ayat et al., 2022; Lengfeld et al., 2020), and numerical model simulations (Fung et al., 2021; Yang et al., 2019, 2021).

In summary, we provide systematic evidence on the exacerbation of rainfall extremes over the areas with higher degree of urbanization in a coastal megalopolis. Such exacerbation is nonlinearly biased towards short (~ 2-year) return periods and short durations (< 6-hour) particularly in urban areas. The tendency of more frequent ‘nuisance’ events may have less dramatic consequences but nonetheless pose recurrent challenges for urban transport and drainage infrastructure (Fowler et al., 2021), which necessitates adaptation to increasing risk of flash floods and protection measures for vulnerable people (Yin et al., 2023). Such level of details is often not of concern at continental-scale and event-based studies owing to coarse resolutions and small sample amount of rainfall records, respectively, but is essential to bridge the gap between atmospheric science and flood hydrology (Westra et al., 2014), and is important to both scientists and decision-makers.

Acknowledgements

This work is financially supported by General Research Fund projects (No. 17202020, No. 17210923) from Hong Kong Research Grants Council, and Environment and Conservation Fund Project (ref: 108/2019) from Hong Kong Environmental Protection Department. X.C. received funding from National Key Research and Development Program of China for Intergovernmental Cooperation (2019YFE0110100), Science and technology innovation team project of Guangdong Meteorological Bureau (GRMCTD202104) and the National Natural Science Foundation of China (41975124).

Conflict of Interest

The authors declare no conflicts of interest.

Data Availability Statement

The hourly precipitation data of rain gauges can be obtained from https://data.cma.cn/data/cdcdetail/dataCode/A.0012.0001.html for Guangdong stations and https://www.hko.gov.hk/tc/cis/reqform.htm for Hong Kong stations. The MSWEP V.2.8 gridded precipitation data are available at http://www.gloh2o.org/mswep/, The IMERG V07 data are available at https://gpm.nasa.gov/data/directory. Era5-Land reanalysis data including hourly gridded precipitation, surface (2m above ground) temperature and dew point temperature were obtained from https://cds.climate.copernicus.eu/#!/search?text=ERA5&type=dataset. The FABDEM terrain data was sourced from https://data.bris.ac.uk/data/dataset/25wfy0f9ukoge2gs7a5mqpq2j7. Land cover data including the Greater Bay Area were obtained from https://www.resdc.cn/doi/doi.aspx?DOIid=54. The MCS datasets can be accessed from https://doi.pangaea.de/10.1594/PANGAEA.877914 and https://zenodo.org/record/6534163#.Y9j0XnbP0uU. The International Best Track Archive for Climate Stewardship (IBTrACS) can be obtained at https://www.ncei.noaa.gov/products/international-best-track-archive. The merged and corrected gridded hourly precipitation dataset over the GBA, as well as scripts for data processing and analysis, can be accessed in the Zenodo repository https://zenodo.org/record/7948722.

References

Agilan, V., & Umamahesh, N. V. (2015). Detection and attribution of non-stationarity in intensity and frequency of daily and 4-h extreme rainfall of Hyderabad, India. *Journal of Hydrology*, *530*, 677–697. https://doi.org/10.1016/j.jhydrol.2015.10.028

Agilan, V., & Umamahesh, N. V. (2016). Is the covariate based non-stationary rainfall IDF curve capable of encompassing future rainfall changes? *Journal of Hydrology*, *541*, 1441–1455. https://doi.org/10.1016/j.jhydrol.2016.08.052

Alexander, L. V., Fowler, H. J., Bador, M., Behrangi, A., Donat, M. G., Dunn, R., Funk, C., Goldie, J., Lewis, E., Rogé, M., Seneviratne, S. I., & Venugopal, V. (2019). On the use of indices to study extreme precipitation on sub-daily and daily timescales. *Environmental Research Letters*, *14*(12), 125008. https://doi.org/10.1088/1748-9326/ab51b6

Ali, H., Fowler, H. J., Lenderink, G., Lewis, E., & Pritchard, D. (2021). Consistent Large-Scale Response of Hourly Extreme Precipitation to Temperature Variation Over Land. *Geophysical Research Letters*, *48*(4). https://doi.org/10.1029/2020GL090317

Ayat, H., Evans, J. P., Sherwood, S. C., & Soderholm, J. (2022). Intensification of subhourly heavy rainfall. *Science*, *378*(6620), 655–659. https://doi.org/10.1126/science.abn8657

Baez-Villanueva, O. M., Zambrano-Bigiarini, M., Beck, H. E., McNamara, I., Ribbe, L., Nauditt, A., Birkel, C., Verbist, K., Giraldo-Osorio, J. D., & Xuan Thinh, N. (2020). RF-MEP: A novel Random Forest method for merging gridded precipitation products and ground-based measurements. *Remote Sensing of Environment*, *239*, 111606. https://doi.org/10.1016/j.rse.2019.111606

Bao, J., Sherwood, S. C., Alexander, L. V., & Evans, J. P. (2017). Future increases in extreme precipitation exceed observed scaling rates. *Nature Climate Change*, *7*(2), 128–132. https://doi.org/10.1038/nclimate3201

Barbero, R., Fowler, H. J., Lenderink, G., & Blenkinsop, S. (2017). Is the intensification of precipitation extremes with global warming better detected at hourly than daily resolutions? *Geophysical Research Letters*, 10.

Beck, H. E., Wood, E. F., Pan, M., Fisher, C. K., Miralles, D. G., van Dijk, A. I. J. M., McVicar, T. R., & Adler, R. F. (2019). MSWEP V2 Global 3-Hourly 0.1° Precipitation: Methodology and Quantitative Assessment. *Bulletin of the American Meteorological Society*, *100*(3), 473–500. https://doi.org/10.1175/BAMS-D-17-0138.1

Berg, P., Moseley, C., & Haerter, J. O. (2013). Strong increase in convective precipitation in response to higher temperatures. *Nature Geoscience*, *6*(3), 181–185. https://doi.org/10.1038/ngeo1731

Chan, S. C., Kendon, E. J., Roberts, N. M., Fowler, H. J., & Blenkinsop, S. (2016). Downturn in scaling of UK extreme rainfall with temperature for future hottest days. *Nature Geoscience*, *9*(1), 24–28. https://doi.org/10.1038/ngeo2596

Chand, S. S., Walsh, K. J. E., Camargo, S. J., Kossin, J. P., Tory, K. J., Wehner, M. F., Chan, J. C. L., Klotzbach, P. J., Dowdy, A. J., Bell, S. S., Ramsay, H. A., & Murakami, H. (2022).

Declining tropical cyclone frequency under global warming. *Nature Climate Change*, *12*(7), 655–661. https://doi.org/10.1038/s41558-022-01388-4

Chang, C., Chen, Y., & Huang, J. J. (2023). A comparison study on the role of urbanization in altering the short-duration and long-duration intense rainfall. *Science of The Total Environment*, *857*, 159290. https://doi.org/10.1016/j.scitotenv.2022.159290

Chen, D., Guo, J., Yao, D., Lin, Y., Zhao, C., Min, M., Xu, H., Liu, L., Huang, X., Chen, T., & Zhai, P. (2019). Mesoscale Convective Systems in the Asian Monsoon Region From Advanced Himawari Imager: Algorithms and Preliminary Results. *Journal of Geophysical Research: Atmospheres*, *124*(4), 2210–2234. https://doi.org/10.1029/2018JD029707

Chen, Y., Liao, Z., Shi, Y., Tian, Y., & Zhai, P. (2021). Detectable Increases in Sequential Flood-Heatwave Events Across China During 1961–2018. *Geophysical Research Letters*, *48*(6). https://doi.org/10.1029/2021GL092549

Chen, Y.-R., Yu, B., & Jenkins, G. (2013). Secular variation in rainfall and intensity–frequency–duration curves in Eastern Australia. *Journal of Water and Climate Change*, *4*(3), 244–251. https://doi.org/10.2166/wcc.2013.138

Cheng, T. F., Dong, Q., Dai, L., & Lu, M. (2022). A Dual Regime of Mesoscale Convective Systems in the East Asian Monsoon Annual Cycle. *Journal of Geophysical Research: Atmospheres*, *127*(13). https://doi.org/10.1029/2022JD036523

Coles, S., Pericchi, L. R., & Sisson, S. (2003). A fully probabilistic approach to extreme rainfall modeling. *Journal of Hydrology*, *273*(1–4), 35–50. https://doi.org/10.1016/S0022-1694(02)00353-0

Fauer, F. S., & Rust, H. W. (2022). *Non-Stationary Large-Scale Statistics of Precipitation Extremes in Central Europe* (arXiv:2211.04140). arXiv. http://arxiv.org/abs/2211.04140

Fischer, E. M., & Knutti, R. (2016). Observed heavy precipitation increase confirms theory and early models. *Nature Climate Change*, *6*(11), 986–991. https://doi.org/10.1038/nclimate3110

Fowler, H. J., Lenderink, G., Prein, A. F., Westra, S., Allan, R. P., Ban, N., Barbero, R., Berg, P., Blenkinsop, S., Do, H. X., Guerreiro, S., Haerter, J. O., Kendon, E. J., Lewis, E., Schaer, C., Sharma, A., Villarini, G., Wasko, C., & Zhang, X. (2021). Anthropogenic intensification of short-duration rainfall extremes. *Nature Reviews Earth & Environment*, *2*(2), 107–122. https://doi.org/10.1038/s43017-020-00128-6

Fu, G., Chiew, F. H., Zheng, H., Robertson, D. E., Potter, N. J., Teng, J., Post, D. A., Charles, S. P., & Zhang, L. (2021). Statistical analysis of attributions of climatic characteristics to nonstationary rainfall-streamflow relationship. *Journal of Hydrology*, *603*, 127017. https://doi.org/10.1016/j.jhydrol.2021.127017

Fung, K. Y., Tam, C., Lee, T. C., & Wang, Z. (2021). Comparing the Influence of Global Warming and Urban Anthropogenic Heat on Extreme Precipitation in Urbanized Pearl River Delta Area Based on Dynamical Downscaling. *Journal of Geophysical Research: Atmospheres*, *126*(21). https://doi.org/10.1029/2021JD035047

Ganguli, P., & Coulibaly, P. (2017). Does nonstationarity in rainfall require nonstationary intensity–duration–frequency curves? *Hydrology and Earth System Sciences*, *21*(12), 6461–6483. https://doi.org/10.5194/hess-21-6461-2017

Gocic, M., & Trajkovic, S. (2013). Analysis of changes in meteorological variables using Mann-Kendall and Sen's slope estimator statistical tests in Serbia. *Global and Planetary Change*, *100*, 172–182. https://doi.org/10.1016/j.gloplacha.2012.10.014

Grimm, N. B., Faeth, S. H., Golubiewski, N. E., Redman, C. L., Wu, J., Bai, X., & Briggs, J. M. (2008). Global Change and the Ecology of Cities. *Science*, *319*(5864), 756–760. https://doi.org/10.1126/science.1150195

Hall, T. M., & Kossin, J. P. (2019). Hurricane stalling along the North American coast and implications for rainfall. *Npj Climate and Atmospheric Science*, *2*(1), 17. https://doi.org/10.1038/s41612-019-0074-8

Han, J.-Y., Baik, J.-J., & Lee, H. (2014). Urban impacts on precipitation. *Asia-Pacific Journal of Atmospheric Sciences*, *50*(1), 17–30. https://doi.org/10.1007/s13143-014-0016-7

Hersbach, H., Bell, B., Berrisford, P., Hirahara, S., Horányi, A., Muñoz-Sabater, J., Nicolas, J., Peubey, C., Radu, R., Schepers, D., Simmons, A., Soci, C., Abdalla, S., Abellan, X., Balsamo, G., Bechtold, P., Biavati, G., Bidlot, J., Bonavita, M., … Thépaut, J. (2020). The ERA5 global reanalysis. *Quarterly Journal of the Royal Meteorological Society*, *146*(730), 1999–2049. https://doi.org/10.1002/qj.3803

Hosseinzadehtalaei, P., Tabari, H., & Willems, P. (2020). Climate change impact on short-duration extreme precipitation and intensity–duration–frequency curves over Europe. *Journal of Hydrology*, *590*, 125249. https://doi.org/10.1016/j.jhydrol.2020.125249

Huang, J., Fatichi, S., Mascaro, G., Manoli, G., & Peleg, N. (2022). Intensification of sub-daily rainfall extremes in a low-rise urban area. *Urban Climate*, *42*, 101124. https://doi.org/10.1016/j.uclim.2022.101124

Huang, X., Hu, C., Huang, X., Chu, Y., Tseng, Y., Zhang, G. J., & Lin, Y. (2018). A long-term tropical mesoscale convective systems dataset based on a novel objective automatic tracking algorithm. *Climate Dynamics*, *51*(7–8), 3145–3159. https://doi.org/10.1007/s00382-018-4071-0

Huffman, G. J., Bolvin, D. T., Joyce, R., Nelkin, E. J., Tan, J., Hsu, K., Kelley, O. A., Nguyen, P., Watters, D. C., West, B. J., & Xie, P. (2023). *NASA Global Precipitation Measurement (GPM) Integrated Multi-satellitE Retrievals for GPM (IMERG) Version 07*. https://gpm.nasa.gov/sites/default/files/2023-07/IMERG_V07_ATBD_final_230712.pdf

IPCC. (2021). *Climate Change 2021: The Physical Science Basis. Contribution of Working Group I to the Sixth Assessment Report of the Intergovernmental Panel on Climate Change [Masson-Delmotte, V., P. Zhai, A. Pirani, S.L. Connors, C. Péan, S. Berger, N. Caud, Y. Chen, L. Goldfarb, M.I. Gomis, M. Huang, K. Leitzell, E. Lonnoy, J.B.R. Matthews, T.K. Maycock, T. Waterfield, O. Yelekçi, R. Yu, and B. Zhou (eds.)]*.

Khaliq, M. N., Ouarda, T. B. M. J., Gachon, P., Sushama, L., & St-Hilaire, A. (2009). Identification of hydrological trends in the presence of serial and cross correlations: A review of selected methods and their application to annual flow regimes of Canadian rivers. *Journal of Hydrology*, *368*(1–4), 117–130. https://doi.org/10.1016/j.jhydrol.2009.01.035

Khaliq, M. N., Ouarda, T. B. M. J., Ondo, J.-C., Gachon, P., & Bobée, B. (2006). Frequency analysis of a sequence of dependent and/or non-stationary hydro-meteorological observations: A review. *Journal of Hydrology*, *329*(3–4), 534–552. https://doi.org/10.1016/j.jhydrol.2006.03.004

Kidd, C., Becker, A., Huffman, G. J., Muller, C. L., Joe, P., Skofronick-Jackson, G., & Kirschbaum, D. B. (2017). So, How Much of the Earth's Surface Is Covered by Rain Gauges? *Bulletin of the American Meteorological Society*, *98*(1), 69–78. https://doi.org/10.1175/BAMS-D-14-00283.1

Lai, Y., Li, J., Gu, X., Chen, Y. D., Kong, D., Gan, T. Y., Liu, M., Li, Q., & Wu, G. (2020). Greater flood risks in response to slowdown of tropical cyclones over the coast of China. *Proceedings of the National Academy of Sciences*, *117*(26), 14751–14755. https://doi.org/10.1073/pnas.1918987117

Lenderink, G., & van Meijgaard, E. (2008). Increase in hourly precipitation extremes beyond expectations from temperature changes. *Nature Geoscience*, *1*(8), 511–514. https://doi.org/10.1038/ngeo262

Lengfeld, K., Kirstetter, P.-E., Fowler, H. J., Yu, J., Becker, A., Flamig, Z., & Gourley, J. (2020). Use of radar data for characterizing extreme precipitation at fine scales and short durations. *Environmental Research Letters*, *15*(8), 085003. https://doi.org/10.1088/1748-9326/ab98b4

Li, P., Moseley, C., Prein, A. F., Chen, H., Li, J., Furtado, K., & Zhou, T. (2020). Mesoscale Convective System Precipitation Characteristics over East Asia. Part I: Regional Differences and Seasonal Variations. *Journal of Climate*, *33*(21), 9271–9286. https://doi.org/10.1175/JCLI-D-20-0072.1

Li, Y., Fowler, H. J., Argüeso, D., Blenkinsop, S., Evans, J. P., Lenderink, G., Yan, X., Guerreiro, S. B., Lewis, E., & Li, X. (2020). Strong Intensification of Hourly Rainfall Extremes by Urbanization. *Geophysical Research Letters*, *47*(14). https://doi.org/10.1029/2020GL088758

Lin, L., Gao, T., Luo, M., Ge, E., Yang, Y., Liu, Z., Zhao, Y., & Ning, G. (2020). Contribution of urbanization to the changes in extreme climate events in urban agglomerations across China. *Science of The Total Environment*, *744*, 140264. https://doi.org/10.1016/j.scitotenv.2020.140264

Liu, J., & Niyogi, D. (2019). Meta-analysis of urbanization impact on rainfall modification. *Scientific Reports*, *9*(1), 7301. https://doi.org/10.1038/s41598-019-42494-2

Liu, L., & Wang, Y. (2020). Trends in Landfalling Tropical Cyclone–Induced Precipitation over China. *Journal of Climate*, *33*(6), 2223–2235. https://doi.org/10.1175/JCLI-D-19-0693.1

McLeod, J., & Shepherd, M. (2022). A Synoptic Framework for Forecasting the Urban Rainfall Effect Using Composite and K-Means Cluster Analyses. *Frontiers in Environmental Science*, *10*, 808026. https://doi.org/10.3389/fenvs.2022.808026

McLeod, J., Shepherd, M., & Konrad, C. E. (2017). Spatio-temporal rainfall patterns around Atlanta, Georgia and possible relationships to urban land cover. *Urban Climate*, *21*, 27–42. https://doi.org/10.1016/j.uclim.2017.03.004

Milly, P. C. D., Betancourt, J., Falkenmark, M., Hirsch, R. M., Kundzewicz, Z. W., Lettenmaier, D. P., & Stouffer, R. J. (2008). *Stationarity Is Dead: Whither Water Management? 319*. https://doi.org/10.1126/science.1151915

Naylor, J., & Mulholland, J. P. (2023). The Impact of Vertical Wind Shear on the Outcome of Interactions Between Squall Lines and Cities. *Journal of Geophysical Research: Atmospheres*, *128*(3), e2022JD037237. https://doi.org/10.1029/2022JD037237

Nerantzaki, S. D., & Papalexiou, S. M. (2022). Assessing extremes in hydroclimatology: A review on probabilistic methods. *Journal of Hydrology*, *605*, 127302. https://doi.org/10.1016/j.jhydrol.2021.127302

Oh, S.-G., Son, S.-W., & Min, S.-K. (2021). Possible impact of urbanization on extreme precipitation–temperature relationship in East Asian megacities. *Weather and Climate Extremes*, *34*, 100401. https://doi.org/10.1016/j.wace.2021.100401

Papalexiou, S. M., & Montanari, A. (2019). Global and Regional Increase of Precipitation Extremes Under Global Warming. *Water Resources Research*, *55*(6), 4901–4914. https://doi.org/10.1029/2018WR024067

Qiang, Y., Zhang, L., & Xiao, T. (2020). Spatial-temporal rain field generation for the Guangdong-Hong Kong-Macau Greater Bay Area considering climate change. *Journal of Hydrology*, *583*, 124584. https://doi.org/10.1016/j.jhydrol.2020.124584

Sarhadi, A., & Soulis, E. D. (2017). Time-varying extreme rainfall intensity-duration-frequency curves in a changing climate. *Geophysical Research Letters*, *44*(5), 2454–2463. https://doi.org/10.1002/2016GL072201

Schelske, O., Sundermann, L., & Hausmann, P. (2013). *Mind the risk—A global ranking of cities under threat from natural disasters*. Swiss Re.

Shepherd, J. M. (2013). Impacts of Urbanization on Precipitation and Storms: Physical Insights and Vulnerabilities. In *Climate Vulnerability* (pp. 109–125). Elsevier. https://doi.org/10.1016/B978-0-12-384703-4.00503-7

Shepherd, J. M., Carter, M., Manyin, M., Messen, D., & Burian, S. (2010). The Impact of Urbanization on Current and Future Coastal Precipitation: A Case Study for Houston. *Environment and Planning B: Planning and Design*, *37*(2), 284–304. https://doi.org/10.1068/b34102t

Shepherd, J. M., Pierce, H., & Negri, A. J. (2002). Rainfall Modification by Major Urban Areas: Observations from Spaceborne Rain Radar on the TRMM Satellite. *Journal of Applied Meteorology*, *41*(7), 689–701. https://doi.org/10.1175/1520-0450(2002)041<0689:RMBMUA>2.0.CO;2

Slater, L. J., Anderson, B., Buechel, M., Dadson, S., Han, S., Harrigan, S., Kelder, T., Kowal, K., Lees, T., Matthews, T., Murphy, C., & Wilby, R. L. (2021). Nonstationary weather and water extremes: A review of methods for their detection, attribution, and management. *Hydrology and Earth System Sciences*, *25*(7), 3897–3935. https://doi.org/10.5194/hess-25-3897-2021

Song, F., Zhang, G. J., Ramanathan, V., & Leung, L. R. (2022). Trends in surface equivalent potential temperature: A more comprehensive metric for global warming and weather extremes. *Proceedings of the National Academy of Sciences*, *119*(6), e2117832119. https://doi.org/10.1073/pnas.2117832119

Sun, Q., Miao, C., Duan, Q., Ashouri, H., Sorooshian, S., & Hsu, K. (2018). A Review of Global Precipitation Data Sets: Data Sources, Estimation, and Intercomparisons. *Reviews of Geophysics*, *56*(1), 79–107. https://doi.org/10.1002/2017RG000574

Sun, X., Luo, Y., Gao, X., Wu, M., Li, M., Huang, L., Zhang, D.-L., & Xu, H. (2021). On the Localized Extreme Rainfall over the Great Bay Area in South China with Complex Topography and Strong UHI Effects. *Monthly Weather Review*, *149*(8), 2777–2801. https://doi.org/10.1175/MWR-D-21-0004.1

Sun, X., & Wang, G. (2022). Causes for the Negative Scaling of Extreme Precipitation at High Temperatures. *Journal of Climate*, *35*(18), 6119–6134. https://doi.org/10.1175/JCLI-D-22-0142.1

Tang, Y., Huang, A., Wu, P., Huang, D., Xue, D., & Wu, Y. (2021). Drivers of Summer Extreme Precipitation Events Over East China. *Geophysical Research Letters*, *48*(11). https://doi.org/10.1029/2021GL093670

Visser, J. B., Wasko, C., Sharma, A., & Nathan, R. (2021). Eliminating the “hook” in Precipitation-Temperature Scaling. *Journal of Climate*, 1–42. https://doi.org/10.1175/JCLI-D-21-0292.1

Vu, T. M., & Mishra, A. K. (2019). Nonstationary frequency analysis of the recent extreme precipitation events in the United States. *Journal of Hydrology*, *575*, 999–1010. https://doi.org/10.1016/j.jhydrol.2019.05.090

Westra, S., Alexander, L. V., & Zwiers, F. W. (2013). Global Increasing Trends in Annual Maximum Daily Precipitation. *Journal of Climate*, *26*(11), 3904–3918. https://doi.org/10.1175/JCLI-D-12-00502.1

Westra, S., Fowler, H. J., Evans, J. P., Alexander, L. V., Berg, P., Johnson, F., Kendon, E. J., Lenderink, G., & Roberts, N. M. (2014). Future changes to the intensity and frequency of short-duration extreme rainfall: FUTURE INTENSITY OF SUB-DAILY RAINFALL. *Reviews of Geophysics*, *52*(3), 522–555. https://doi.org/10.1002/2014RG000464

Westra, S., & Sisson, S. A. (2011). Detection of non-stationarity in precipitation extremes using a max-stable process model. *Journal of Hydrology*, *406*(1–2), 119–128. https://doi.org/10.1016/j.jhydrol.2011.06.014

Yamaguchi, M., Chan, J. C. L., Moon, I.-J., Yoshida, K., & Mizuta, R. (2020). Global warming changes tropical cyclone translation speed. *Nature Communications*, *11*(1), 47. https://doi.org/10.1038/s41467-019-13902-y

Yan, H., Guan, M., & Kong, Y. (2023). Flood Retention Lakes in a Rural-Urban Catchment: Climate-Dominated and Configuration-Affected Performances. *Water Resources Research*, *59*(8), e2022WR032911. https://doi.org/10.1029/2022WR032911

Yang, L., Ni, G., Tian, F., & Niyogi, D. (2021). Urbanization Exacerbated Rainfall Over European Suburbs Under a Warming Climate. *Geophysical Research Letters*, *48*(21). https://doi.org/10.1029/2021GL095987

Yang, L., Smith, J., & Niyogi, D. (2019). Urban Impacts on Extreme Monsoon Rainfall and Flooding in Complex Terrain. *Geophysical Research Letters*, *46*(11), 5918–5927. https://doi.org/10.1029/2019GL083363

Yilmaz, A. G., Hossain, I., & Perera, B. J. C. (2014). Effect of climate change and variability on extreme rainfall intensity–frequency–duration relationships: A case study of Melbourne. *Hydrology and Earth System Sciences*, *18*(10), 4065–4076. https://doi.org/10.5194/hess-18-4065-2014

Yin, J., Gao, Y., Chen, R., Yu, D., Wilby, R., Wright, N., Ge, Y., Bricker, J., Gong, H., & Guan, M. (2023). Flash floods: Why are more of them devastating the world's driest regions? *Nature*, *615*(7951), 212–215. https://doi.org/10.1038/d41586-023-00626-9

Zhang, J., Xu, J., Dai, X., Ruan, H., Liu, X., & Jing, W. (2022). Multi-Source Precipitation Data Merging for Heavy Rainfall Events Based on Cokriging and Machine Learning Methods. *Remote Sensing*, *14*(7), 1750. https://doi.org/10.3390/rs14071750

Zhang, L., Cheng, T. F., Lu, M., Xiong, R., & Gan, J. (2023). Tropical Cyclone Stalling Shifts Northward and Brings Increasing Flood Risks to East Asian Coast. *Geophysical Research Letters*, *50*(10), e2022GL102509. https://doi.org/10.1029/2022GL102509